1000-0569/2015/031(07)-2053-62 *Acta Petrologica Sinica* 岩石学报

西藏冈底斯南缘雄村铜金矿床成矿斑岩厘定及其锆石 U-Pb 和黑云母 Ar-Ar 年龄分析*

邹银桥[1,2] 黄文婷[1] 梁华英[1**] 伍静[3] 林书平[1,2] 王秀璋[1]

ZOU YinQiao[1,2], HUANG WenTing[1], LIANG HuaYing[1**], WU Jing[3], LIN ShuPing[1,2] and WANG XiuZhang[1]

1. 中国科学院广州地球化学研究所,中国科学院矿物学与成矿学重点实验室,广州 510640
2. 中国科学院大学,北京 100049
3. 广西大学资源与冶金学院,南宁 530004
1. *CAS Key Laboratory of Mineralogy and Metallogeny, Guangzhou Institute of Geochemistry, Chinese Academy of Sciences, Guangzhou* 510640, *China*
2. *University of Chinese Academy of Sciences, Beijing* 100049, *China*
3. *College of Resources and Metallurgy of Guangxi University, Nanning* 530004, *China*

2014-09-22 收稿, 2014-12-18 改回.

Zou YQ, Huang WT, Liang HY, Wu J, Lin SP and Wang XZ. 2015. Identification of porphyry genetically associated with mineralization and its zircon U-Pb and biotite Ar-Ar age of the Xiongcun Cu-Au deposit, southern Gangdese, Tibet. *Acta Petrologica Sinica*, 31(7):2053－2062

Abstract The Xiongcun super-large Cu-Au porphyry deposit occurs as veinlet and disseminated mineralization in strongly altered rocks. There are different opinions on the type of ore bearing rock due to that the rocks underwent strongly alteration and therefore, protolith could not easily be recognized. The mineral assemblage and structure of the ore-hosted rocks are systematically studied through thin section identification at the relatively weakly altered domains. It is found at the weakly domain of the thin section that the protolith was characterized by porphyritic texture. The phenocrysts are dominantly plagioclase, K-feldspars, and minor quarts, while matrix is consist of K-feldspar and plagioclase. The petrology features indicate they are mainly of quartz syenite porphyry and a small amount of monzonite porphyry. Based on our work, together with previous work, it is concluded that the strongly altered ore bearing rocks include mainly quartz syenite porphyry, volcanic rocks and some monzonite porphyry. The Xiongcun quartz syenite porphyry underwent potassic alteration, silication, and magnetic alteration, which is common in the early stage alteration of Cu-Au porphyry deposits all over the world. The Xiongcun quartz has high zircon Ce^{4+}/Ce^{3+} ratios, with an average of 1169, suggesting that the magma of the Xiongcun syenite porphyry was formed under high oxygen fugacity, which was the same as those found in most of the porphyry Cu-Au deposits in the world. The alteration assemblage in the quartz syenite porphyry and the high oxygen fugacity of the magma of syenite porphyry suggest that the quartz syenite porphyry is genetically related to the Xiongcun Cu-Au mineralizatoin. Quartz syenite porphyry has zircon LA-ICP-MS U-Pb age of 173.7 ± 2.1Ma, with MSWD = 0.23 and Ar-Ar age of biotite formed by potassic alteration in the quartz syenite porphyry is 48.3 ± 0.9Ma, with MSWD = 1.58. The biotite Ar-Ar age is much younger than the zircon U-Pb age and on the other hand, is coeval with the age of granitic batholith located in northeastern Xiongcun Cu-Au ore field, suggesting that biotite ^{40}Ar-^{39}Ar isotope system was reset by subsequent magma event. It is concluded that the quartz syenite porphyry is genetically related to Xiongcun Cu-Au mineralization and that the Xiongcun porphyry deposit was formed by the northward subduction of Neo-Tethys. The Ar-Ar age of biotite formed by potassic alteration can't record the mineralization age of the porphyry deposit due to its Ar-Ar isotope system was reset by later thermal events.

Key words Xiongcun; Zircon U-Pb dating; Porphyry Cu-Au deposit; Neo-Tethys; Southern Gangdese

---

* 本文受中国科学院战略性先导科技专项(B类)(XDB03010302)和国家自然科学基金项目(41121002、41172080、40772054)联合资助.

第一作者简介: 邹银桥,男,1991年生,博士生,矿床学专业,E-mail: 554604088@qq.com

** **通讯作者:** 梁华英,男,1962年生,研究员,博士生导师,矿床地质及矿床地球化学专业,E-mail: lianghy@gig.ac.cn

摘　要　雄村特大型斑岩铜金矿床主要以细脉浸染状产于强烈蚀变岩石中,赋矿岩石原岩成因类型存在争议。本文对多个赋矿蚀变岩石作了系统光薄片显微鉴定,在多个蚀变较弱的矿化样品中发现赋矿岩石具斑状结构,其基质主要为钾长石,斑晶主要为斜长石、钾长石及少量石英,显示石英正长斑岩及二长斑岩(少量)矿物组成特征。结合前人工作,可以认为雄村铜金矿床赋矿岩石为正长斑岩、火山岩及少量二长斑岩。正长斑岩发育斑岩铜金矿床成矿早期常见的钾硅化蚀变及磁铁矿化蚀变,锆石具高的 Ce^{4+}/Ce^{3+} 比值(334~3084,平均值为 1169),显示高氧逸度岩浆特征,和世界斑岩铜金矿床成矿岩体一致;这表明石英正长斑岩为雄村铜金矿床成矿岩体。石英正长斑岩锆石 LA-ICP-MS U-Pb 年龄为 173.7±2.1Ma(MSWD=0.23),石英正长斑岩钾化阶段形成的黑云母 $^{40}Ar/^{39}Ar$ 坪年龄为 48.3±0.9Ma(MSWD=1.58),远小于锆石 U-Pb 年龄却与矿区东北部始新世花岗岩基的年龄一致,显示 Ar-Ar 年龄受后期地质事件影响而发生重置。通过上述研究,可以认为雄村铜金矿床为与石英正长斑岩有关的斑岩型矿床,形成时代约 173Ma,和新特提斯洋洋壳向北俯冲诱发的岩浆事件有关,矿区内云母受后期地质事件影响重置,不能记录其形成时代。

关键词　雄村;锆石 U-Pb 年龄;斑岩型铜金矿床;新特提斯;冈底斯南缘

中图法分类号　P588.133;P597.3

冈底斯带记录了特提斯洋的打开消亡及欧亚大陆碰撞的重要地质事件(Chung *et al.*, 2005, 2009; Mo *et al.*, 2005, 2007; Royden *et al.*, 2008; Zhu *et al.*, 2013),同时是我国重要的斑岩铜矿产出地带(侯增谦等, 2001, 2004; Yang *et al.*, 2009)。因此,冈底斯带南缘岩浆及矿床形成引起地质学家的重视。现有研究表明,冈底斯带南缘斑岩铜钼矿床主要形成于碰撞后(<65Ma)的造山环境。雄村铜金矿床位于日喀则地区谢通门县,探明铜储量大于 100 万吨,金大于 100 吨(郎兴海等, 2012),是冈底斯南缘发现的首个俯冲期与中酸性岩浆作用有关的矿床。雄村铜金矿床的发现引起了人们广泛关注,开展了大量工作(Qin *et al.*, 2005; Tafti, 2006; Tafti *et al.*, 2009; 徐文艺等, 2006a, b; 郎兴海等, 2010b, 2011, 2013; 应丽娟等, 2012; 曲晓明等, 2007a; 唐菊兴等, 2009a, b, 2010; Lang *et al.*, 2014)。郎兴海等(2012)获得矿床辉钼矿 Re-Os 同位素模式年龄在 160~163Ma,提出矿床形成于俯冲构造环境;郎兴海等(2011)、应立娟等(2012)分析了矿床蚀变-物化探元素分布地质特征,此外对矿区内各地质体的年代学及地球化学特征(曲晓明等, 2007a; 唐菊兴等, 2009a, b, 2010; Tafti, 2006; Tafti *et al.*, 2009; 郎兴海等, 2010b, 2013)及成矿流体特征也开展了较多的研究工作(徐文艺等, 2006b)。雄村铜金矿床主要为浸染状产于强硅化蚀变中酸性火成岩中,矿体为厚板状,具有斑岩型矿床的矿化特征,又和典型斑岩矿床的不同。由于赋矿岩石发生强烈蚀变,原岩特征及成因类型不易识别,因而对赋矿岩石类型及矿床成因类型有不同看法。主要有赋矿岩石为白垩纪海底火山碎屑岩,矿床为火山块状硫化物矿床(Qin *et al.*, 2005);赋矿岩石为新生代火山岩,矿床为新生代未发育成熟的斑岩矿化与浅成低温热液矿床(徐文艺等, 2006a);破碎带蚀变岩型铜金矿床(曲晓明等, 2007b);赋矿岩石为侏罗纪闪长玢岩,矿床为斑岩型矿床(Lang *et al.*, 2014; 唐菊兴等, 2010)等。因此,分析蚀变赋矿岩石成因类型,对了解本矿床形成过程及成因类型有着重要的意义。本文在详细观察分析雄村矿区赋矿岩石显微特征的基础上,分析赋矿岩石成因类型、岩浆特征、锆石 LA-ICP-MS U-Pb 年龄及蚀变黑云母 Ar-Ar 年龄,借此讨论矿床的成因类型及形成背景。

1　矿区地质概况及矿床地质特征

雄村斑岩铜金矿床位于西藏日喀则地区谢通门县荣玛乡雄村,大地构造位置为西藏冈底斯成矿带中段南缘,南侧紧邻日喀则弧前盆地(图 1)(徐文艺等, 2006b; 唐菊兴等, 2009b)。

矿区出露的地层主要为一套酸性-安山质凝灰岩、凝灰质砂岩及泥页岩和全新统崩积物-冲积物(唐菊兴等, 2009a; 应立娟等, 2012)。过去认为其为白垩纪海相火山岩(Qin *et al.*, 2005),近年来随着凝灰岩锆石 U-Pb 年龄(176~195Ma)测定(唐菊兴等, 2010; 曲晓明等,2007a),现多认为其为中下侏罗统凝灰质火山沉积岩。

矿区岩浆活动强烈,主要有出露于矿区东部的始新世黑云母钾长花岗岩及矿区西部及南部的中晚侏罗世(角闪)石英闪长玢岩(图 1)。矿区东部黑云母钾长花岗岩为区域上的花岗岩大岩基,岩体新鲜无矿化,为白垩纪-古近纪南冈底斯岩基的组成部分,常呈岩脉状侵入其西部的侏罗纪地质体和雄村铜金矿体中(唐菊兴等, 2010)。

矿区断裂构造发育,主要呈北西向、北西西向或北北西向展布,沿断层普遍分布有断层角砾岩和构造蚀变岩。次级断层呈北西或北北西走向,大多具有陡倾特点,倾向北东或东,均为成矿后断层(郎兴海等, 2010a, b)。

雄村铜金矿床探明 Cu 储量 >100Mt,平均品位为 0.45%,Au >100t,平均品位 0.61g/t。矿体为厚板状,长轴北西向,长约 1200 多米,宽约 600m,平均厚度大于 200m(唐菊兴等, 2009b)。主要金属矿物为:黄铜矿、黄铁矿、闪锌矿、磁铁矿及自然金等。非金属矿物主要为石英、红柱石、钾长石、斜长石、绢云母、黑云母等(郎兴海, 2012)。

矿体经历了很强的热液蚀变作用,主要有钾化、硅化、绢云母化、泥化、绿泥石-绿帘石化、堇青石化及红柱石化等。赋矿岩石硅化较强,多处见强硅化形成的硅化岩。

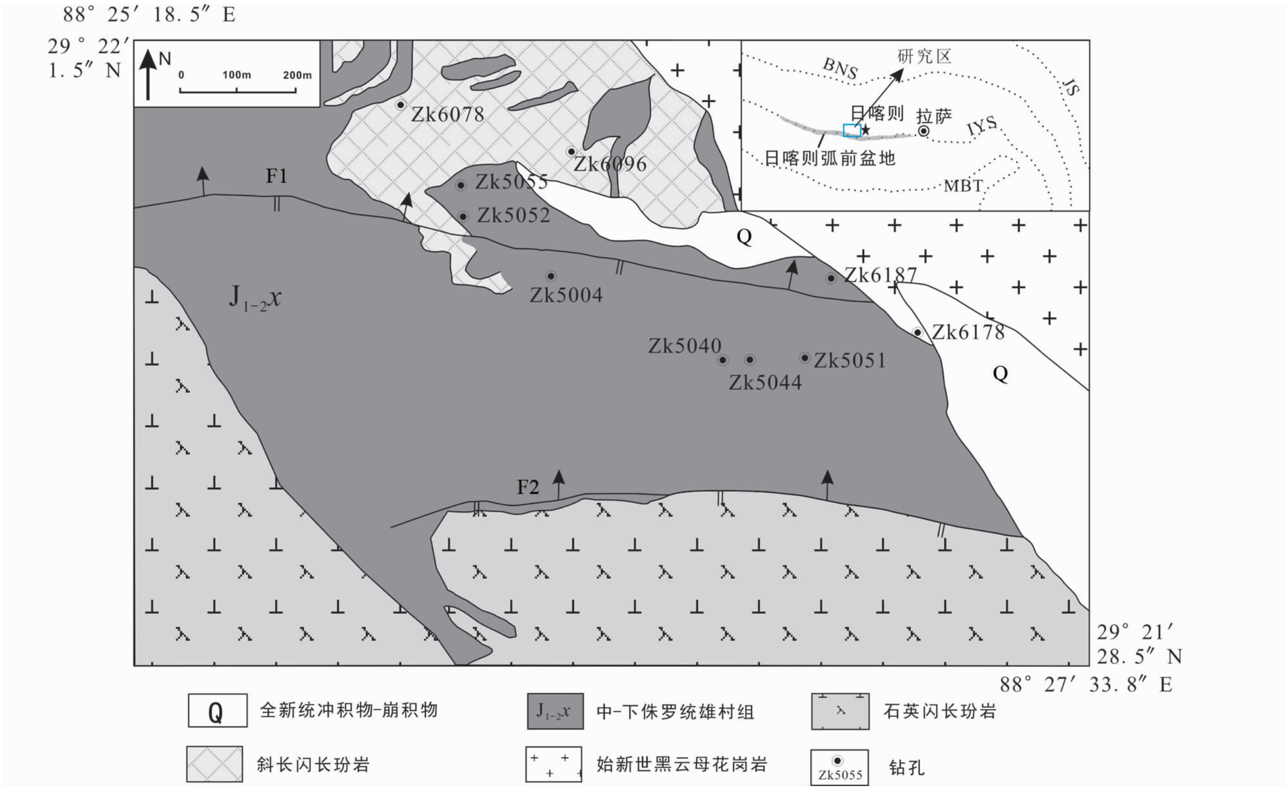

图 1 雄村斑岩铜金矿床矿区地质图(据郎兴海等,2010a 修编)

Fig. 1 Geological map of Xiongcun porphyry Cu-Au deposit (modified after Lang *et al.*, 2010a)

2 雄村矿化岩石特征及成因类型分析

为了分析雄村铜金矿床赋矿岩石类型,我们对雄村铜金矿床多个钻孔矿化岩体作了详细的光薄片观察鉴定。由于雄村铜金矿床赋矿岩石发生了强烈蚀变,多数原岩被蚀变破坏,因而只能通过蚀变岩石局部蚀变较弱部位矿物组成分析岩石类型。我们在雄村矿区 ZK5004、ZK5040、ZK5042、ZK5044、ZK5052、ZK5055、ZK6178(图 1)7 个钻孔不同深度采样,对矿化岩石作了系统的光薄片观察鉴定,多数样品已发生强烈硅化而形成硅化岩,少数局部蚀变较弱部位显微特征见图 2。

在 ZK6178 孔 169.4m 处,岩石具斑状结构,斑晶主要由斜长石,牌号 An = 12 ~ 21 之间,为更长石(已绢云母化)和钾长石组成(图 2a),见浑圆状石英斑晶(图 2b),基质主要由钾长石、斜长石组成;该岩石结构及矿物组成特征表明其为二长斑岩。其余 ZK5004、ZK5040、ZK5042、ZK5044、ZK5052、ZK5055 6 个钻孔的赋矿蚀变岩石具斑状结构,斑晶主要由斜长石(An 为 2 ~ 3,为钠长石)、钾长石(图 2c, e)及较少石英组成(图 2g),基质主要为钾长石(图 2f),粒度多在 2mm 左右,显示石英正长斑岩的特征。上述赋矿蚀变岩石矿物组成及结构特征表明其主要为石英正长斑岩-石英二长斑岩。石英正长斑岩和石英二长斑岩矿化蚀变特征一致可能属同一岩石系列。雄村铜金矿床部分矿化还产于火山岩中,因此,雄村铜金矿床赋矿岩石主要为石英正长斑岩、二长斑岩及火山岩。

石英正长斑岩中普遍见斑岩型铜金矿床成矿早期常见的钾硅化及磁铁矿化蚀变,局部见钾化形成的细粒状黑云母(图 2d, e)和浸染状铜矿化共生及浸染状磁铁矿(图 3h)。雄村铜金矿床正长斑岩中见堇青石(图 2f, g)。正长斑岩中堇青石应该是岩浆上升至浅部地壳过程中捕获的铝质泥岩(围岩)形成的。

3 分析方法

3.1 锆石 LA-ICP-MS U-Pb 同位素组成及微量元素分析

样品采自 ZK5005 孔 312m 处,矿化石英正长斑岩(XC7-12)用常规方法粉碎至 60 目,用水初步淘选之后经过磁选精选,在双目镜下手工挑选出自形的晶型较好的锆石。将待测锆石置于环氧树脂中制成靶、磨至约一半使锆石中心部位暴露并抛光,然后进行反射光、透射光照相。利用阴极发光(CL)扫描电镜进行图像分析确定单颗粒锆石的形态、结构,以选择颗粒大、较自形清晰无包体的锆石进行分析。

阴极发光(CL)图像在西北大学大陆动力学国家重点实验室拍摄完成。锆石原位微区 LA-ICP-MS U-Pb 定年及锆石微量元素分析在广州地球化学研究所同位素地球化学国家

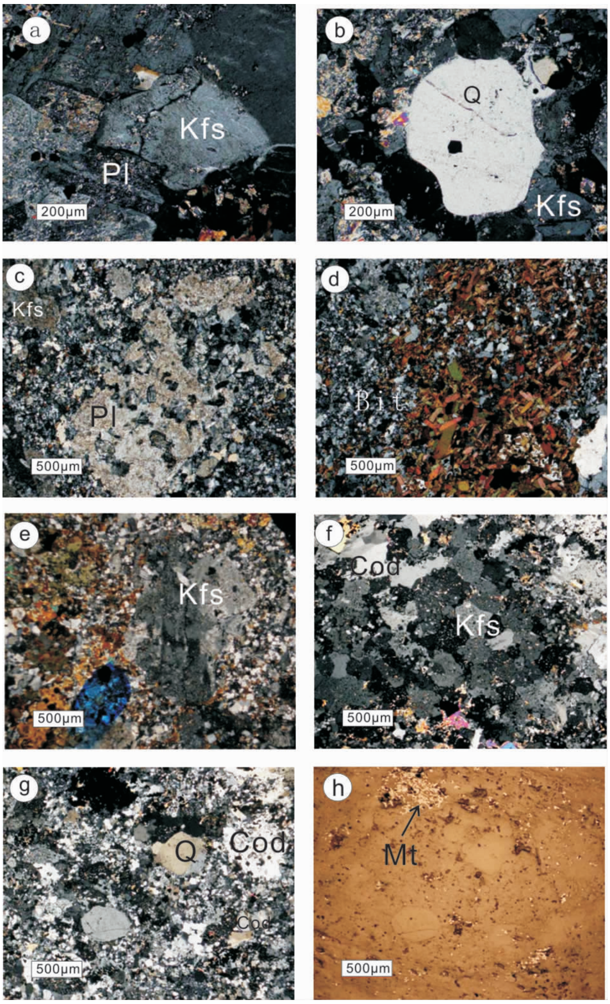

图 2 雄村铜金矿床赋矿岩石显微特征图

Pl-斜长石;Kfs-钾长石;Cod-堇青石;Mt-磁铁矿;Bit-黑云母

Fig. 2 Microphotographs of ore-bearing porphyry of Xiongcun Cu-Au deposit

Pl-plagioclase; Kfs-K-feldspar; Cod-cordierite; Mt-magnetite; Bit-biotite

重点实验室进行。分析使用 Resolution M-50 激光剥蚀系统和 Agilent 7500a 型的 ICP-MS 联机的 LA-ICP-MS。使用标准锆石 TEMORA 及微量元素标样 NIST 610。微量元素含量计算以 Si 为内标、NIST610 为外标。具体仪器组成和实验参数参考文献(Li *et al.*, 2012; Ding *et al.*, 2013)。对分析数据的离线处理,包括对样品的信号选择、仪器灵敏度漂移校正、元素含量及 U-Th-Pb 同位素比值和年龄计算采用 ICPMSDataCal 7.2 软件(Liu *et al.*, 2010),锆石样品的 U-Pb 年龄谐和图绘制和年龄加权平均年龄计算采用 ISOPLOT(Ludwig, 2003)。

锆石 Ce^{4+}/Ce^{3+} 比值通过测定锆石及岩石稀土元素含量计算(Ballard *et al.*, 2002)。为了排除锆石中磷灰石包体及其它地质事件对锆石 Ce^{4+}/Ce^{3+} 比值影响,只计算具有效锆石年龄的 Ce^{4+}/Ce^{3+} 比值。

3.2 黑云母 Ar-Ar 同位素分析

在详细光薄片观察的基础上,选取 Xc7-09(石英正长斑岩)样品黑云母作 Ar-Ar 年龄分析。黑云母与磁铁矿共生(图 2d),偶见星点黄铜矿,表明其为斑岩矿床成矿早期钾硅化及磁铁矿化阶段形成的。样品经破碎至 20 目,在双目显微镜下挑选 0.2g 左右的云母,挑纯至 99%。用纯铝铂纸将样品包裹成直径约 6mm 的球形,与标样 ZBH-25 一同封闭于玻璃瓶中,送至中国原子能科学研究院 49-2 反应堆 B4 孔道进行中子照射,照射时间为 24h,中子通量为(6.0~6.5)× 1012/cm^2·s。用于中子通量监测的样品是我国周口店 K-Ar 标准黑云母(ZBH-25,年龄为 132.7Ma)。照射后的样品冷置后,装入圣诞树状的样品架中,密封去气之后,装入系统。

样品测试 $^{40}Ar/^{39}Ar$ 同位素年代分析在中国科学院广州地球化学研究所同位素地球化学国家重点实验室进行,具体的分析技术规格见(Qiu *et al.*, 2010; Yun *et al.*, 2010)。$^{40}Ar/^{39}Ar$ 定年结果的计算和投点采用 ArArCALC 计算软件(Koppers, 2002; 张凡等, 2009)。

4 分析结果

实验分析了石英正长斑岩的锆石 U-Pb 同位素组成、锆石 Ce^{4+}/Ce^{3+} 比值以及黑云母的 Ar-Ar 同位素组成(表 1、表 2)。含矿石英正长斑岩 LA-ICP-MS U-Pb 年龄在 157 ~ 198Ma 之间,4 个分析点谐和度 < 90%,锆石 Th/U 比值在 0.49~1.10 之间。黑云母主要加热阶段的 Ar-Ar 表观年龄为 38.9~48.8Ma 之间。

5 讨论

5.1 石英正长斑岩岩浆高氧逸度特征及成矿岩体分析

与斑岩铜金矿化有关的岩浆多具有较高的氧逸度。高氧逸度岩浆中的硫为氧化硫,而氧化态硫在岩浆中的溶解度较大,使岩浆中的硫在岩浆形成演化过程中处于不饱和状态,有利于亲铜元素在岩浆形成演化过程中富集形成矿床(Sillitoe, 1997; Mungall, 2002; Ballard *et al.*, 2002; Sun *et al.*, 2004, 2010, 2013, 2014; Liang *et al.*, 2006, 2009)。锆石 Ce^{4+}/Ce^{3+} 比值可反映成矿岩浆氧逸度相对高低,斑岩铜金矿床的成矿岩体锆石多具较高的 Ce^{4+}/Ce^{3+} 比值(Ballard *et al.*, 2002; Liang *et al.*, 2006)。西藏玉龙铜矿的成矿岩体锆石的 Ce^{4+}/Ce^{3+} 一般大于 200,而非成矿岩体则一般小于 120,智利斑岩铜金矿床成矿岩体锆石 Ce^{4+}/Ce^{3+} 值大于 300。雄村赋矿石英正长斑岩的锆石 Ce^{4+}/Ce^{3+} 值大,变化大,在 334 至 3084 之间(表 1),平均 1169,显示石英正长斑岩具高氧逸度特征,和世界斑岩铜金矿床成矿岩体的值相似。这初步显示石英正长斑岩和矿化有内在成因联系。

表 1　含矿石英正长斑岩锆石 LA-ICP-MS 分析结果

Table 1　Zircon LA-ICP-MS data of ore-bearing quartz syenite porphyry

测点号	U ($\times 10^{-6}$)	Th/U	Ce^{4+}/Ce^{3+}	$^{206}Pb/^{238}U$	±1σ	$^{207}Pb/^{235}U$	±1σ	$^{208}Pb/^{232}Th$	±1σ	$^{206}Pb/^{238}U$ Age (Ma)	±1σ	$^{207}Pb/^{235}U$ Age (Ma)	±1σ	谐和度
Xc7-12-01	134	0.59	682	0.02759	0.00099	0.04188	0.02759	0.00909	0.00094	175.4	6.2	173.4	35.9	98%
Xc7-12-02	165	0.52	701	0.03116	0.00092	0.03321	0.03116	0.00975	0.00076	197.8	5.8	197.9	27.8	99%
Xc7-12-03	76	0.49	898	0.03042	0.00157	0.04670	0.03042	0.00824	0.00123	193.2	9.8	191.9	39.3	99%
Xc7-12-04	111	0.58	362	0.02724	0.00114	0.03524	0.02724	0.00856	0.00120	173.2	7.1	160.8	30.6	92%
Xc7-12-05	72	0.47	2932	0.02720	0.00146	0.06116	0.02720	0.01172	0.00145	173.0	9.2	166.1	52.8	95%
Xc7-12-06	63	0.52	214	0.02631	0.00123	0.05251	0.02631	0.01202	0.00182	167.4	7.7	149.7	46.0	88%
Xc7-12-07	175	0.56	3084	0.02765	0.00110	0.02823	0.02765	0.01005	0.00084	175.8	6.9	172.8	24.2	98%
Xc7-12-08	104	0.57	645	0.03037	0.00168	0.14477	0.03037	0.02764	0.00503	192.9	10.5	466.3	93.1	17%
Xc7-12-09	125	0.47	1949	0.02717	0.00115	0.04217	0.02717	0.01071	0.00149	172.8	7.2	180.6	35.9	95%
Xc7-12-10	122	0.62	358	0.03035	0.00129	0.04565	0.03035	0.01411	0.00192	192.7	8.1	193.0	38.3	99%
Xc7-12-11	117	0.67	532	0.02788	0.00113	0.04629	0.02788	0.00864	0.00095	177.3	7.1	176.2	39.5	99%
Xc7-12-12	95	0.53	3045	0.02730	0.00130	0.06492	0.02730	0.01408	0.00184	173.6	8.2	171.7	55.7	98%
Xc7-12-13	119	0.55	536	0.02703	0.00117	0.04666	0.02703	0.01163	0.00113	171.9	7.4	175.4	39.9	97%
Xc7-12-14	318	0.86	1482	0.02469	0.00080	0.02585	0.02469	0.00862	0.00061	157.2	5.0	159.9	22.4	98%
Xc7-12-15	97	1.08	334	0.02781	0.00140	0.07113	0.02781	0.01207	0.00115	176.8	8.8	178.1	60.7	99%
Xc7-12-16	227	0.56	639	0.02734	0.00084	0.02532	0.02734	0.00916	0.00081	173.9	5.3	163.2	21.9	93%
Xc7-12-17	133	0.50	1070	0.03084	0.00154	0.11378	0.03084	0.01830	0.00467	195.8	9.6	414.2	77.0	28%
Xc7-12-18	132	0.51	572	0.02782	0.00158	0.06899	0.02782	0.01095	0.00170	176.9	9.9	166.2	59.5	93%
Xc7-12-19	238	0.66	3361	0.03248	0.00195	0.16083	0.03248	0.03283	0.00658	206.1	12.2	562.0	94.2	7%
Xc7-12-20	117	0.49	605	0.02572	0.00118	0.05861	0.02572	0.00919	0.00116	163.7	7.4	162.7	50.7	99%

表 2　雄村斑岩矿床石英正长斑岩黑云母 $^{40}Ar/^{39}Ar$ 测年结果

Table 2　$^{40}Ar/^{39}Ar$ isotopic age analyses of biotite from Xiongcun ore bearing quartz syenite porphyry

阶段	激光能量	$^{36}Ar(air)$	$^{37}Ar(Ca)$	$^{38}Ar(Cl)$	$^{39}Ar(k)$	$^{40}Ar^*$	Age ±2σ (Ma)		$^{40}Ar^*$ (%)	$^{39}Ar(k)^*$	K/Ca	±2σ	有效
J = 0.00916441 ± 0.00004582, t_p = 48.3 ± 0.89Ma, t_f = 36.15 ± 1.57Ma, t_n = 51.44 ± 11.69Ma, t_i = 51.23 ± 11.63Ma													
1	4.10%	9.21890	67.02099	25.84839	180.85400	91.3742	8.35	± 10.14	3.24	13.26	1.51	± 0.29	
2	4.30%	2.82728	6.11169	9.97807	70.73270	68.8807	16.07	± 8.04	7.61	5.18	6.48	± 15.35	
3	4.50%	2.18296	0.26324	12.02188	86.02310	149.6716	28.61	± 5.00	18.82	6.31	183	± 8288.86	
4	4.70%	0.94415	9.31931	6.02422	44.68100	87.1079	32.02	± 4.22	23.78	3.27	2.68	± 2.89	
5	4.90%	0.48992	18.33820	3.37453	24.77960	47.949	31.79	± 4.20	24.86	1.82	0.76	± 0.56	
6	5.10%	2.69669	49.28639	18.06755	128.12580	263.0632	33.71	± 4.25	24.8	9.39	1.46	± 0.59	
7	5.30%	0.69216	4.72037	6.75919	48.62450	119.4257	40.25	± 2.88	36.83	3.56	5.77	± 17.96	
8	5.50%	0.72354	11.51087	7.85396	54.04340	135.2055	40.99	± 2.78	38.7	3.96	2.63	± 4.32	
9	5.90%	0.25893	0	3.58874	24.82780	65.9262	43.48	± 2.33	46.24	1.82	2.63	± 4.32	
10	6.30%	1.61121	35.71137	25.58804	185.40210	496.0843	43.81	± 1.77	50.97	13.59	2.91	± 1.52	
11	6.90%	0.38736	4.70151	3.80595	28.53770	67.5648	38.82	± 3.08	37.08	2.09	3.4	± 11.82	
12	7.90%	0.33749	7.88930	7.14278	47.30580	131.255	45.41	± 1.77	56.75	3.47	3.36	± 6.66	√
13	9.50%	0.25057	10.13475	9.12390	55.17990	159.9179	47.4	± 1.25	68.26	4.04	3.05	± 3.23	√
14	14.50%	0.70453	21.98175	26.12612	187.29730	553.9066	48.36	± 0.94	72.58	13.73	4.77	± 3.26	√
15	19.50%	0.53041	13.70952	17.75968	128.36410	383.2632	48.82	± 1.00	70.87	9.41	5.24	± 3.71	√
16	30.00%	0.98716	0	9.38607	69.54500	185.5319	43.68	± 2.85	38.84	5.1	5.24	± 3.71	

注：J 为无量纲照射参数；t_p 为有效坪年龄；t_f 为全熔年龄；t_n 为等时线年龄；t_i 为反等时线年龄；"√"代表用于计算样品有效坪年龄的数据

斑岩矿床成矿岩体多发育成矿早期钾硅化及磁铁矿化（Liang *et al.*, 2009），雄村铜金矿床赋矿石英正长斑岩发育斑岩铜（金）矿床早期常见的钾硅化（图 2d, e）及磁铁矿化-硅化（图 2h）等蚀变。这也表明石英正长斑岩与铜金矿化有成因联系。

雄村赋矿石英正长斑岩高氧逸度岩浆特征及蚀变特征表明石英正长斑岩与铜金矿化具有内在成因关系，雄村铜金矿床为与石英正长斑岩有关的斑岩型矿床。

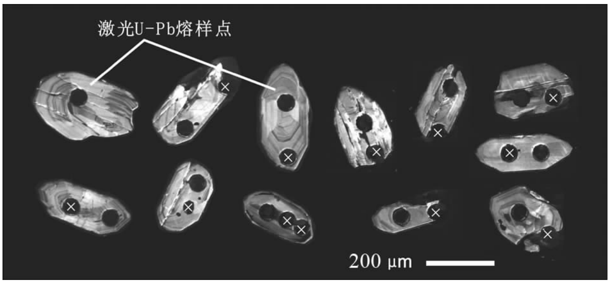

图 3 雄村斑岩矿床赋矿石英正长斑岩锆石 CL 图

Fig. 3 CL images of the analyzed zircon grains from the ore-bearing quartz syenite porphyry, Xiongcun porphyry deposit

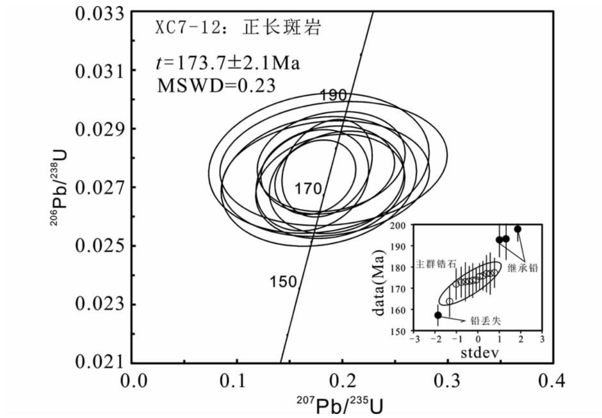

图 4 雄村斑岩矿床赋矿石英正长斑岩锆石 $^{206}Pb/^{238}U$-$^{207}Pb/^{235}U$ 年龄谐和图（内插图为累计概率统计图）

Fig. 4 Concordia plot showing the zircon U-Pb analyses of the ore-bearing quartz-syenite porphyry of the Xiongcun porphyry deposit (the insert is probability plot)

5.2 石英正长斑岩形成时代

锆石阴极发光图像（图 3）显示，测试样品锆石多为自形-半自形柱状，晶体为无色-淡褐色，长轴方向 200 ~ 300μm，长宽比在 1 ~ 3 之间，振荡环带发育，锆石 Th/U 值大于 0.5（表 1），表明测定的锆石为岩浆结晶成因锆石（Hoskin and Black, 2000）。

本次实验共测定 20 颗锆石样品的 T-U-Pb 同位素组成，其中 4 个点谐和度在 90% 以下，不参与计算。其余 16 颗锆石 $^{238}U/^{206}Pb$ 年龄在 157 ~ 198Ma 之间。为减少继承铅、铅丢失对年龄的影响，我们用累计概率统计图处理锆石 $^{206}Pb/^{238}U$ 年龄数据（图 4 内插图）。在累积概率统计图上，岩体主群锆石多为直线分布，直线上方分布点视作继承 Pb，直线下方分布点视作 Pb 丢失（Harris *et al.*, 2004）。雄村斑岩铜金矿床石英正长斑岩锆石 16 个分析点中，3 个较大年龄点和 1 个较小年龄点明显不在直线上，分别视作继承铅和铅丢失，其余 12 个点获得主群锆石加权平均年龄为 173.7 ± 2.1Ma，MSWD = 0.23。锆石 U-Pb 同位素封闭温度较高，主群锆石年龄代表岩体的结晶年龄（Harris *et al.*, 2004）。因此，雄村石英正长斑岩形成时代为 173.7 ± 2.1Ma。

5.3 黑云母 Ar-Ar 年龄及后期热事件的影响分析

矿区东部大面积出露新生代钾长花岗岩，而矿区钻孔中也见大量晚期脉岩。前人据绢云母 Ar-Ar 年龄约为 38Ma 左右，提出矿床是新生代形成的浅成低温矿床（徐文艺等, 2006a, b）。为了分析后期岩浆热事件对该区成矿的影响，我们分析了斑岩铜金矿床钾化阶段形成的黑云母（图 2d）Ar-Ar 年龄（表 2）。黑云母样品共进行了 16 个阶段的激光加热阶段，年龄谱及坪年龄见图 5a，所有数据点对应的正反等时线年龄图见图 5b, c。分析结果显示，表观年龄呈阶梯状递增，变化范围从 8.4 ~ 48.8Ma，总气体年龄 36.2 ± 1.6Ma。在激光加热前 6 个阶段表面年龄由 8.4Ma 增至 33.7Ma（图 5a），^{39}Ar 仅为析出量的 28%，后十个加热阶段表观年龄在 38.9 ~ 48.8Ma，并在激光加热第 13 ~ 16 阶段取得了似坪年龄为 48.3 ± 0.9Ma（图 5a）。所有数据点对应的正反等时线年龄分别为 51.4 ± 11.7Ma, 51.2 ± 11.6Ma（图 5b, c），其初始 $^{40}Ar/^{36}Ar$ 为 247.4 ± 177（图 5b），略小于大气 $^{40}Ar/^{36}Ar$（295.5）。在本文中用坪年龄代表黑云母 Ar-Ar 同位素记录的时代。

本文获得的斑岩矿床钾化阶段黑云母 Ar-Ar 坪年龄（48.3 ± 0.9Ma）远远小于石英正长斑岩锆石 U-Pb 同位素年龄（173.7 ± 2.1Ma），而和矿区东部始新世花岗岩大岩基（46.5 ± 1.1Ma）、穿插矿体黑云母花岗闪长岩岩脉（46.9 ± 0.4Ma）及云煌岩脉（49.6 ± 0.6Ma）（唐菊兴等, 2009a, 2010）等一致。这表明雄村斑岩型铜金矿床受后期强烈地质热事件的干扰，斑岩矿床钾化阶段形成黑云母 Ar-Ar 同位素体系由于受到后期地质热事件的影响而发生重置，仅记录后期地质热事件而不能反映其形成时代。

现有研究成果表明，斑岩铜矿床成岩成矿系统时间跨度约 1Myr 左右（Cathles *et al.*, 1997；梁华英等, 2008, 2009）。雄村斑岩型矿床成矿岩体锆石 U-Pb 年龄（173.7 ± 2.1Ma）和郎兴海等（2012）辉钼矿 Re-Os 模式年龄（161.5 ± 2.7Ma）存在较大的差异，相差约 12Ma。石英正长斑岩蚀变特征及高氧逸度岩浆特征表明其为成矿岩体，那么为什么辉钼矿模式年龄和岩体存在约 12Ma 时差？我们认为雄村斑岩铜金矿床两种同位素体系年龄差异较大，可能主要是下列两个原因所致：

其一是辉钼矿后受到后期地质热事件的影响，导致 Re-Os 年龄变小。前人研究表明辉钼矿中的 Re 在中低温流体或表生条件下易发生迁移丢失或在辉钼矿中微粒 K-Si 矿物如伊利石中富集，导致辉钼矿 Re-Os 年龄异常大或变小，前者如美国内华达州 Gold Acres 矽卡岩型 Cu-Mo 矿床，后者如纳米比亚 Lorelei 斑岩 Cu-Mo 矿床（McCandless *et al.*, 1993）。雄村斑岩矿床受后期地质事件强烈影响，发生强烈硅化及泥化蚀变，斑岩矿床钾化阶段黑云母 Ar-Ar 同位素体

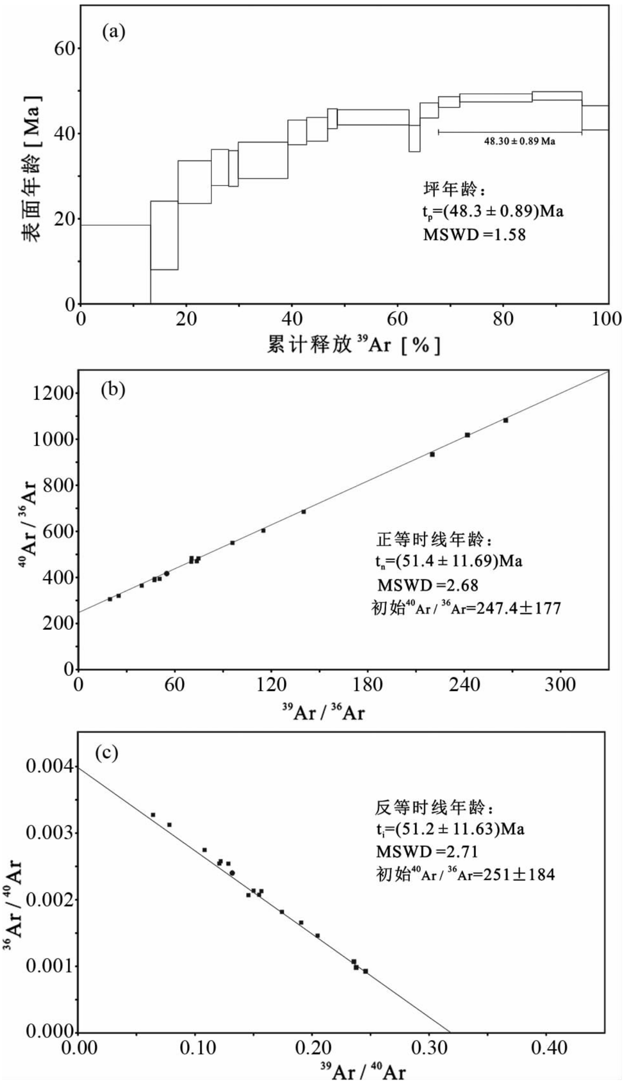

图 5 正长斑岩中蚀变黑云母^{40}Ar-^{39}Ar 坪年龄和等时线年龄

Fig. 5 The ^{40}Ar-^{39}Ar age plateaus and isochrones for biotite from ore-bearing rock of Xiongcun porphyry deposit

系也由于受后期地质事件扰动而发生重置；Os 一般比较稳定（McCandless *et al.*, 1993），因此，雄村斑岩型铜金矿床辉钼矿 Re-Os 年龄远小于成矿岩体锆石 U-Pb 年龄可能是辉钼矿在后期蚀变作用下，辉钼矿中微粒粘土矿物获得外来 Re 所致。其二可能是辉钼矿分析点较少，4 个点在等时线上主要集于 2 区域（朗兴海等, 2012），等时线年龄误差较大。

5.4 矿床形成的构造背景及过程分析

冈底斯带为班-怒缝合带与雅江缝合带之间的巨型构造岩浆岩带，记录了新特提斯洋的打开与消亡的构造演化（Chung *et al.*, 2005；Zhu *et al.*, 2013；Royden *et al.*, 2008）以及陆陆碰撞造山作用等主要地质事件（Mo *et al.*, 2005, 2007；Chung *et al.*, 2009）。已有资料表明，新特提斯洋打开时间不晚于晚三叠世（Mo *et al.*, 2007, 2008），现已发现的冈底斯南缘桑日群火山岩年龄最老为 195Ma，显示典型的岛弧火山岩的地球化学特征（Kang *et al.*, 2014），表明新特提斯洋开始俯冲的时间不晚于早侏罗世。目前在冈底斯南缘发现了一系列形成于早中侏罗世，与洋壳俯冲有关的火成岩（Harrison *et al.*, 1992；Chu *et al.*, 2006；Ji *et al.*, 2009；董彦辉等, 2006；张宏飞等, 2007；Tafti *et al.*, 2009；唐菊兴等, 2010；曲晓明等, 2007a），表明新特提斯洋壳至少在早侏罗世开始向北俯冲，在冈底斯南缘引发了强烈的火山岩浆活动，形成冈底斯岩浆弧及日喀则弧前盆地。一般认为，特提斯洋于 65Ma 闭合，两个大陆开始碰撞（Mo *et al.*, 2007, 2008；Ding *et al.*, 2005）。因此，冈底斯南缘形成时代大于 65Ma 小于 195Ma 的岩浆岩及有关矿床多与新特提斯洋壳俯冲背景有关。雄村斑岩铜金矿床位于冈底斯南缘日喀则弧前盆地，成矿岩体石英正长斑岩锆石 LA-ICP-MS U-Pb 年龄为 173.7±2.1Ma，MSWD=0.23，因此，雄村斑岩型铜金矿床的形成与新特提斯洋向北俯冲有关。锆石 Hf 同位素组成表明（将在另文中发表），石英正长斑岩 $\varepsilon_{Hf}(t)$ 在 11～15 之间，显新生地壳特征。据冈底斯南缘中生代构造背景，初步认为雄村斑岩铜金矿床形成过程可概括为，新特提斯洋壳在晚三叠纪或早中侏罗纪向北俯冲，俯冲洋壳脱水，交代上覆地幔楔，诱发其部分熔融形成富水高氧逸度钾质岩浆，富水高氧化岩浆分解地幔源区中硫化物，形成富铜金富水高氧化岩浆。成矿岩浆在 173Ma 左右发生侵入岩浆活动，成矿岩浆在上升过程中出溶挥发相，成矿元素 Cu、Au 等由于在流体和熔体中之间分配系数较大，进入岩浆出溶挥发相中；当岩浆上升定位到地壳浅部时，岩浆热液在斑岩体顶部及其围岩接触带附近交代岩体及围岩形成斑岩矿床（Sillitoe, 1972）。

斑岩矿床形成深度一般较浅，多在 1～3km 左右（Cooke *et al.*, 2004），冈底斯带由于后期碰撞引起的地壳加厚、抬升剥蚀等，较先形成的斑岩型矿床遭受破坏而不利于保存。冈底斯南缘大面积出露白垩纪以后岩基，多数斑岩已被剥蚀破坏，因此，冈底斯南缘俯冲型斑岩铜金矿床重点找矿靶区应集中在冈底斯南缘中生代以后凹陷盆地如侏罗纪火山岩分布区。

6 结论

（1）雄村铜金矿床强蚀变赋矿岩石为正长斑岩、火山岩及少量二长斑岩；

（2）石英正长斑岩发育典型的钾化及磁铁矿化蚀变，且具高氧逸度岩浆特征，为成矿岩体；雄村铜金矿床为与石英正长斑岩有关斑岩型矿床；

（3）石英正长斑岩的锆石 LA-ICP-MS U-Pb 年龄为 173.7±2.1Ma，MSWD=0.23，斑岩矿床钾硅化蚀变黑云母 Ar-Ar 坪年龄年龄为 48.3±0.9Ma；雄村斑岩矿床形成与早中侏罗世新特提斯洋北向俯冲诱发岩浆活动有关，云母 Ar-Ar 年龄

受后期热事件影响,不能记录矿床形成时代。

References

Ballard JR, Palin JM and Campbell IH. 2002. Relative oxidation states of magmas inferred from Ce(IV)/Ce(III) in zircon: Application to porphyry copper deposits of northern Chile. Contributions to Mineralogy and Petrology, 144(3): 347 – 364

Cathles LM, Erendi AHJ and Barrie T. 1997. How long can a hydrothermal system be sustained by a single intrusive event? Economic Geology, 92(7 – 8): 766 – 771

Chu MF, Chung SL, Song B, Liu DY, Suzanne YOR, Norman JP, JJ and Wen DJ. 2006. Zircon U-Pb and Hf isotope constraints on the Mesozoic tectonics and crustal evolution of southern Tibet. Geology, 34(9): 745 – 748

Chung SL, Chu MF, Zhang YQ, Xie YW, Lo CH, Lee TY, Lan CY, Li XH, Zhang Q and Wang YZ. 2005. Tibetan tectonic evolution inferred from spatial and temporal variations in post-collisional magmatism. Earth-Science Reviews, 68(3 – 4): 173 – 196

Chung SL, Chu MF, Ji JQ, O'Reilly SY, Pearson NJ, Liu DY, Lee TY and Lo TH. 2009. The nature and timing of crustal thickening in Southern Tibet: Geochemical and zircon Hf isotopic constraints from post-collisional adakites. Tectonophysics, 477(1 – 2): 36 – 48

Cooke DR, Wilson AJ and Davies AGS. 2004. Characteristics and genesis of porphyry copper-gold deposits. University of Tasmania, Centre for Ore Deposit Research Special Publication, 5: 17 – 34

Dong YH, Xu JF, Zeng QG, Wang Q, Mao GZ and Li J. 2006. Is ther a Neo-tethys' subduction record earlier than arc volcanic rocks in the Sangri Group? Acta Petrologica Sinica, 22(3): 661 – 668 (in Chinese with English abstract)

Ding L, Kapp P and Wan XQ. 2005. Paleocene-Eocene record of ophiolite obduction and initial India-Asia collision, southcentral Tibet. Tectonics, 24(3): 1 – 18

Ding X, Hu YH, Zhang H, Li CY, Ling MX and Sun WD. 2013. Major Nb/Ta fractionation recorded in garnet amphibolite facies metagabbro. The Journal of Geology, 121(3): 255 – 274

Harris AC, Allen CM, Bryan SE, Campbell IH, Holcombe RJ and Plain MJ. 2004. ELA-ICP-MS U-Pb zircon geochronology of regional volcanism hosting the Bajo de la Alumbrera Cu-Au deposit: Implications for porphyry-related mineralization. Mineralium Deposita, 39(1): 46 – 67

Harrison TM, Copeland Peter, Kidd WSF and Yin A. 1992. Raising Tibet. Science, 255(5052): 1663 – 1670

Hou ZQ, Qu XM, Huang W and Gao YF. 2001. Gangdise porphyry copper metallogenic belt: The possible second "Yulong" copper belt. Geology in China, 28(10): 27 – 30 (in Chinese with English abstract)

Hou ZQ, Gao YF, Meng XJ, Qu XM and Huang W. 2004. Genesis of adakitic porphyry and tectonic controls on the Gangdese Miocene porphyry copper belt in the Tibetan orogen. Acta Petrologica Sinica, 20(2): 239 – 248 (in Chinese with English abstract)

Hoskin PWO and Black LP. 2010. Metamorphic zircon formation by solid-state recrystallization of protolith igneous zircon. Journal of Metamorphic Geology, 18(4): 423 – 439

Ji WQ, Wu FY, Chung SL, Li JX and Liu CZ. 2009. Zircon U-Pb geochronology and Hf isotopic constraints on petrogenesis of the Gangdese batholith, southern Tibet. Chemical Geology, 262(3 – 4): 229 – 245

Koppers AAP. 2002. ArArCALC-software for $^{40}Ar/^{39}Ar$ age calculations. Computers & Geosciences, 28(5): 605 – 619

Kang ZQ, Xu JF, Simo AW, Feng ZH, Chen JL, Wang BD, Fu WC and Pan HB. 2014. Geochronology and geochemistry of the Sangri Group volcanic rocks, Southern Lhasa terrane: Implications for the early subduction history of the Neo-Tethys and Gangdese magmatic arc. Lithos, 200 – 201: 157 – 168

Lang XH, Chen YC, Tang JX, Li ZJ, Deng Q, Huang Y, Chen Y and Zhang L. 2010a. A discussion on genesis of Xiongcun porphyry copper-gold deposit, Xietongmen, Tibet: Evidences from elements spatial distribution characteristics. Geological Review, 56(3): 384 – 402 (in Chinese with English abstract)

Lang XH, Chen YC, Tang JX, Li ZJ, Huang Y, Wang CH, Chen Y and Zhang L. 2010b. Characteristics of rock geochemistry of orebody No. I in the Xiongcun porphyry copper-gold metallogenic district Xietongmen County, Tibet: Constraints on metallogenic tectonic settings. Geology and Exploration, 46(5): 887 – 898 (in Chinese with English abstract)

Lang XH, Tang JX, Li ZD, Huang Y, Chen Y and Zhang L. 2011. Alteration and mineralization of No. I orebody in Xiongcun porphyry copper-gold metallogenic ore district, Xietongmen County, Tibet. Mineral Deposits, 30(2): 327 – 338 (in Chinese with English abstract)

Lang XH. 2012. Metallogenesis and metallogenic prediction for Xiongcun porphyry copper-gold district, Tibet. Ph. D. Dissertation. Chengdu: Chengdu University of Technology, 53 – 73 (in Chinese with English summary)

Lang XH, Tang JX, Chen YC, Li ZD, Huang Y, Wang CH, Chen Y, Zhang L and Zhou Y. 2012. Neo-Tethys mineralization on the southern margin of the Gangdise metallogenic belt, Tibet, China: Evidence from Re-Os ages of Xiongcun orebody No. I. Earth Science, 37(3): 515 – 525 (in Chinese with English abstract)

Lang XH, Tang JX, Li ZJ, Xie FW and Huang Y. 2013. Jurassic metallogenic event of Gangdese porphyry copper belt in Xiongcun deposit, Tibet: Evidences of geochronology by zircon U-Pb and molybdenite Re-Os isotope. Acta Mineralogica Sinica, 33(Suppl. 2): 328 – 329 (in Chinese)

Lang XH, Tang JX, Li ZJ, Huang Y, Ding F, Yang HH, Xie FW, Zhang L, Wang Q and Zhou Y. 2014. U-Pb and Re-Os geochronological evidence for the Jurassic porphyry metallogenic event of the Xiongcun district in the Gangdese porphyry copper belt, southern Tibet, PRC, Journal of Asian Earth Sciences, 79: 608 – 622

Li H, Ling MX, Li CY, Zhang H, Ding X, Yang XY, Fan WM, Li YL and Sun WD. 2012. A-type granite belts of two chemical subgroups in central eastern China: Indication of ridge subduction. Lithos, 150: 26 – 36

Liang HY, Campbell IH, Allen C, Sun WD, Liu CQ, Yu HX, Xie YW and Zhang YQ. 2006. Zircon Ce^{4+}/Ce^{3+} ratios and ages for Yulong ore-bearing porphyries in eastern Tibet. Mineralium Deposita, 41(2): 152 – 159

Liang HY, Mo JH, Sun WD, Yu HX, Zhang YQ and Allen CM. 2008. Study on the duration of the ore-forming system of the Yulong giant porphyry copper deposit in eastern Tibet, China. Acta Petrologica Sinica, 24(10): 2352 – 2358 (in Chinese with English abstract)

Liang HY, Sun WD, Su WC and Zartman RE. 2009. Porphyry copper-gold mineralization at Yulong, China, promoted by decreasing redox potential during magnetite alteration. Economic Geology, 104(4): 587 – 596

Liang HY, Mo JH, Sun WD, Zhang YQ, Zeng T, Hu GQ and Allen CM. 2009. Study on geochemical composition and isotope ages of the Malasongduo porphyry associated with Cu-Mo mineralization. Acta Petrologica Sinica, 25(2): 385 – 392 (in Chinese with English abstract)

Liu YS, HU ZC, Zong KQ, Gao CG, Gao S, Xu J and Chen HH. 2010. Reappraisement and refinement of zircon U-Pb isotope and trace element analyses by LA-ICP-MS. Chinese Science Bulletin, 55(15): 1535 – 1546

Ludwig KR. 2003. ISOPLOT 3.0: A geochronological toolkit for Microsoft excel. Berkeley: Berkeley Geochronology Center, California

Mungall JE. 2002. Roasting the mantle: Slab melting and the genesis of major Au and Au-rich Cu deposits. Geology, 30(10): 915 – 918

McCandless TE, Ruiz J and Campbell AR. 1993. Rhenium behavior in molybdenite in hypogene and near surface environments: Implications for Re-Os geochronometry. Geochimica et Cosmochimica

Acta, 57(4): 889 - 905

Mo XX, Dong GC, Zhao ZD, Guo TY, Wang LL and Chen T. 2005. Timing of magma mixing in the Gangdisêmagmatic belt during the India-Asia collision: Zircon SHIRMP U-Pb dating. Acta Geologica Sinica, 79(1): 66 - 76

Mo XX, Hou ZQ, Niu YL, Dong GC, Qu XM, Zhao ZD and Yang ZM. 2007. Mantle contributions to crustal thickening during continental collision: Evidence from Cenozoic igneous rocks in southern Tibet. Lithos, 96(1 - 2): 225 - 242

Mo XX, Niu YL, Dong GC, Zhao ZD, Hou ZQ, Zhou S and Ke S. 2008. Contribution of syncollisional felsic magmatism to continental crust growth: A case study of the Paleogene Linzizong volcanic succession in southern Tibet. Chemical Geology, 250(1 - 4): 49 - 67

Qin KZ, Li GM, Li JX, Ding KS and Xie YH. 2005. The Xiongcun Cu-Zn-Au deposit in the western segment of the Gangdese, Tibet: A Mesozoic VHMS-type deposit cut by late veins. Mineral Deposit Research: Meeting the Global Challenge, 1255 - 1258

Qiu HN, Wijbrans JR, Brouwer FM, Yun JB, Zhao LH and Xu YG. 2010. Amphibolite facies retrograde metamorphism of the Zhujiachong eclogite, SE Dabieshan: $^{40}Ar/^{39}Ar$ age constraints from argon extraction using UV-laser microprobe, in vacuo crushing and stepwise heating. Journal of Metamorphic Geology, 28(5): 477 - 487

Qu XM, Xin HB and Xu WY. 2007a. Collation of age of ore-hosting volcanics in Xiongcun superlarge Cu-Au deposit on basis of three zircon U-Pb SHRIMP ages. Mineral Deposits, 26(5): 512 - 518 (in Chinese with English abstract)

Qu XM, Xin HB and Xu WY. 2007b. Petrogenesis of the ore-hosting volcanic rocks and their contribution to mineralization in Xiongcun superlarge Cu-Au deposit, Tibet. Acta Geologica Sinica, 81(7): 965 - 971 (in Chinese with English abstract)

Royden LH, Burchfiel BC and Robert DH. 2008. The geological evolution of the Tibetan Plateau. Science, 321(5892): 1054 - 1058

Sillitoe RH. 1972. A plate tectonic model for the origin of porphyry copper deposits. Economic Geology, 67(2): 184 - 197

Sillitoe RH. 1997. Characteristics and controls of the largest porphyry copper-gold and epithermal gold deposits in the circum-Pacific region. Australian Journal of Earth Sciences, 44(3): 373 - 388

Sun WD, Arculus RJ, Kamenetsky VS and Binns RA. 2004. Release of gold-bearing fluids in convergent margin magmas prompted by magnetite crystallization. Nature, 431(7011): 975 - 978

Sun WD, Ling MX, Yang XY, Fan WM, Ding X and Liang HY. 2010. Ridge subduction and porphyry copper-gold mineralization: An overview. Science China (Earth Sciences), 53(4): 475 - 484

Sun WD, Liang HY, Ling MX, Zhan MZ, Ding, X, Zhang H, Yang XY, Li YL, Ireland TR, Wei QR and Fan WM. 2013. The link between reduced porphyry copper deposits and oxidized magmas. Geochimica et Cosmochimica Acta, 103: 263 - 275

Sun WD, Huang RF, Liang HY, Ling MX, Li CY, Ding X, Zhang H, Yang XY, Trevor I and Fan WM. 2014. Magnetite-hematite, oxygen fugacity, adakite and porphyry copper deposits: Reply to Richards. Geochimica et Cosmochimica Acta, 126: 646 - 649

Tafti R. 2006. Preliminary geochronology report for the Xietongmen deposit area. Tibet, China. Private Report to Continental Minerals Corp.

Tafti R, Mortensen JK, Lang JR, Rebaglitim M and Oliver JL. 2009. Jurassic U-Pb and Re-Os ages for the newly discovered Xietongmen Cu-Au porphyry district, Tibet, PRC: Implications for metalogenic epochs in the southern Gangdese belt. Economic Geology, 104(1): 127 - 136

Tang JX, Zhang L, Huang Y, Wang CH, Li ZJ, Deng Q, Lang XH and Wang Y. 2009a. ^{40}Ar-^{39}Ar isotope ages of main geological bodies in Xiongcun copper-gold deposit, Xietongmen County, Tibet, and their geological significance. Mineral Deposits, 28(6): 759 - 769 (in Chinese with English abstract)

Tang JX, Huang Y, Li ZJ, Deng Q, Lang XH, Chen Y and Zhang L. 2009b. Element geochemical characteristics of Xiongcun Cu-Au deposit in Xietongmoin County, Tibet. Mineral Deposits, 28(1): 15 - 28 (in Chinese with English abstract)

Tang JX, Li FJ, Li ZJ, Zhang L, Tang XQ, Deng Q, Lang XH, Huang Y, Yao XF and Wang Y. 2010. Time limit for formation of main geological bodies in Xiongcun copper-gold deposit, Xietongmen County, Tibet: Evidence from zircon U-Pb ages and Re-Os age of molybdenite. Mineral Deposits, 29(3): 461 - 475 (in Chinese with English abstract)

Xu WY, Qu XM, Hou ZQ, Yang ZS, Pan FZ, Cui YH, Chen WS, Yang D and Lian Y. 2006a. The Xiongcun copper-gold deposit in Tibet: Characteristics, genesis, and geodynamic application. Acta Geologica Sinica, 80(9): 1392 - 1407 (in Chinese with English abstract)

Xu WY, Qu XM, Hou ZQ, Yang D, Yang ZS, Cui YH and Chen WS. 2006b. Ore-forming fluid characteristics and genesis of Xiongcun copper-gold deposit in central Gangdese, Tibet. Mineral Deposits, 25(3): 243 - 251 (in Chinese with English abstract)

Yun JB, Shi HS, Zhu JZ, Zhao LH and Qiu HN. 2010. Dating petroleum emplacement by illite $^{40}Ar/^{39}Ar$ laser stepwise heating. AAPG Bulletin, 94(6): 759 - 771

Yang ZM, Hou ZQ, White NC, Chang ZS, Li ZQ and Song YC. 2009. Geology of the post-collisional porphyry copper-molybdenum deposit at Qulong, Tibet. Ore Geology Reviews, 36(1 - 3): 133 - 159

Ying LJ, Tang JX and Huang Y. 2012. Hornfels comparative study of Jiama and Xiongcun copper deposits, Tibet. Mineral Deposits, 31(2): 380 - 390 (in Chinese with English abstract)

Zhang F, Qiu HN, He HY, Yang LK, Su F, Wang Y and Wu L. 2009. Brief introduction to ArArCALC-software for data reduction in $^{40}Ar/^{39}Ar$ geochronology. Geochimica, 38(1): 53 - 56 (in Chinese with English abstract)

Zhang HF, Xu WC, Guo JQ, Zong KQ, Cai HM and Yuan HL. 2007. Zircon U-Pb and Hf isotopic composition of deformed granite in the southern margin of the Gangdese belt, Tibet: Evidence for early Jurassic subduction of Neo-Tethyan oceanic slab. Acta Petrologica Sinica, 23(6): 1347 - 1353 (in Chinese with English abstract)

Zhu DC, Zhao ZD, Niu YL, Dilek Y, Hou ZQ and Mo XX. 2013. The origin and pre-Cenozoic evolution of the Tibetan Plateau. Gondwana Research, 23(4): 1429 - 1454

附中文参考文献

董彦辉，许继峰，曾庆高，王强，毛国政，李杰. 2006. 存在比桑日群弧火山岩更早的新特提斯洋俯冲记录么？岩石学报，22(3)：661 - 668

侯增谦，曲晓明，黄卫，高永丰. 2001. 冈底斯斑岩铜矿成矿带有望成为西藏第二条“玉龙”铜矿带. 中国地质，28(10)：27 - 30

侯增谦，高永丰，孟祥金，曲晓明，黄卫. 2004. 西藏冈底斯中新世斑岩铜矿带：埃达克质斑岩成因与构造控制. 岩石学报，20(2)：239 - 248

郎兴海，陈毓川，唐菊兴，李志军，邓起，黄勇，陈渊，张丽. 2010a. 西藏谢通门县雄村斑岩型铜金矿床成因讨论——来自元素的空间分布特征的证据. 地质论评，56(3)：384 - 402

郎兴海，陈毓川，唐菊兴，李志军，黄勇，王成辉，陈渊，张丽. 2010b. 西藏谢通门县雄村斑岩型铜金矿集区 I 号矿体的岩石地球化学特征：对成矿构造背景的约束. 地质与勘探，46(5)：887 - 898

郎兴海，唐菊兴，李志军，黄勇，陈渊，张丽. 2011. 西藏谢通门县雄村斑岩型铜金矿集区 I 号矿体的蚀变与矿化特征. 矿床地质，30(2)：327 - 338

郎兴海. 2012. 西藏雄村斑岩型铜金矿集区成矿作用与成矿预测. 博士学位论文. 成都：成都理工大学，53 - 73

郎兴海, 唐菊兴, 陈毓川, 李志军, 黄勇, 王成辉, 陈渊, 张丽, 周云. 2012. 西藏冈底斯成矿带南缘新特提斯洋俯冲期成矿作用: 来自雄村矿集区Ⅰ号矿体的Re-Os同位素年龄证据. 地球科学, 37(3): 515-525

郎兴海, 唐菊兴, 李志军, 谢富伟, 黄勇. 2013. 西藏冈底斯斑岩铜矿带雄村矿区侏罗纪成矿作用:来自锆石U-Pb和辉钼矿Re-Os年龄的证据. 矿物学报, 33(S2): 328-329

梁华英, 莫济海, 孙卫东, 喻亨祥, 张玉泉, Allen CM. 2008. 藏东玉龙超大型斑岩铜矿床成岩成矿系统时间跨度分析. 岩石学报, 24(10): 2352-2358

梁华英, 莫济海, 孙卫东, 张玉泉, 曾提, 胡光黔, Allen CM. 2009. 玉龙铜矿带马拉松多斑岩体岩石学及成岩成矿系统年代学分析. 岩石学报, 25(2): 385-392

曲晓明, 辛洪波, 徐文艺. 2007a. 三个锆石U-Pb SHRIMP年龄对雄村特大型铜金矿床容矿火成岩时代的重新厘定. 矿床地质, 26(5): 512-518

曲晓明, 辛洪波, 徐文艺. 2007b. 西藏雄村特大型铜金矿床容矿火山岩的成因及其对成矿的贡献. 地质学报, 81(7): 965-971

唐菊兴, 张丽, 黄勇, 王成辉, 李志军, 邓起, 郎兴海, 王友. 2009a. 西藏谢通门县雄村铜金矿主要地质体的$^{40}Ar/^{39}Ar$年龄及地质意义. 矿床地质, 28(6): 759-769

唐菊兴, 黄勇, 李志军, 邓起, 郎兴海, 陈渊, 张丽. 2009b. 西藏谢通门县雄村铜金矿床元素地球化学特征. 矿床地质, 28(1): 15-28

唐菊兴, 黎风佶, 李志军, 张丽, 唐晓倩, 邓起, 郎兴海, 黄勇, 姚晓峰, 王友. 2010. 西藏谢通门县雄村铜金矿主要地质体形成的时限:锆石U-Pb、辉钼矿Re-Os年龄的证据. 矿床地质, 29(3): 461-475

徐文艺, 曲晓明, 侯增谦, 杨竹森, 潘凤雏, 崔艳合, 陈伟十, 杨丹, 连玉. 2006a. 西藏雄村大型铜金矿床的特征、成因和动力学背景. 地质学报, 80(9): 1392-1407

徐文艺, 曲晓明, 侯增谦, 杨丹, 杨竹森, 崔艳合, 陈伟十. 2006b. 西藏冈底斯中段雄村铜金矿床成矿流体特征与成因探讨. 矿床地质, 25(3): 243-251

应立娟, 唐菊兴, 黄勇. 2012. 西藏甲玛和雄村铜矿区角岩的对比研究. 矿床地质, 31(2): 380-390

张凡, 邱华宁, 贺怀宇, 杨列坤, 苏菲, 王英, 吴林. 2009. $^{40}Ar/^{39}Ar$年代学数据处理软件ArArCALC简介. 地球化学, 38(1): 53-56

张宏飞, 徐旺春, 郭建秋, 宗克清, 蔡宏明, 袁洪林. 2007. 冈底斯南缘变形花岗岩锆石U-Pb年龄和Hf同位素组成:新特提斯洋早侏罗世俯冲作用的证据. 岩石学报, 23(6): 1347-1353